

University of Wisconsin - Madison

MAD/PH/779

UCD-94-12

NUHEP-TH-94-8

April 1994

Production of Weak Bosons and Higgs Bosons in e^-e^- Collisions

V. Barger^a, J.F. Beacom^a, Kingman Cheung^b, and T. Han^c

^a*Physics Department, University of Wisconsin, Madison, WI 53706*

^b*Department of Physics & Astronomy, Northwestern University, Evanston, IL 60208*

^c*Department of Physics, University of California, Davis, CA 95616*

Abstract

We present calculations of cross sections for single W^- and Z production and W^-W^- , W^-Z , $W^- \gamma$, ZZ , and W^+W^- pair production within the Standard Model at e^-e^- linear colliders. We evaluate Standard-Model Higgs boson production in the channels $e^-e^- \rightarrow e^-e^-H$, $e^- \nu W^- H$, and e^-e^-ZH . We also illustrate the enhancements in the W^-W^- cross section that would result from a strongly-interacting Higgs sector or from a H^{--} resonance in a Higgs doublet + triplet model.

1. Introduction

High-energy experiments at e^+e^- colliders have proved to be very fruitful. The measurements at LEP I and SLC give precision tests of the Standard Model for electroweak interactions[1]. In addition, interesting direct limits have been placed on the Higgs boson mass and the masses of supersymmetric and other new particles[2]. As a means to continue to address these important issues, the design of linear e^+e^- colliders with center-of-mass energies in the range 0.3–2.0 TeV is being actively pursued worldwide[3]. With an appropriate design, an e^+e^- collider could also be operated as an e^-e^- collider[4].

The construction of high energy e^-e^- colliders has not been pursued in recent times. The probable reason for this lack of activity is the absence of s -channel resonance production in e^-e^- due to lepton number conservation. However, precisely because direct channel resonances are not expected, high energy e^-e^- collisions could be a clean way to uncover physics beyond the Standard Model (SM), and several new physics signals have recently been discussed[5].

There are a number of interesting physics possibilities for an e^-e^- collider. In the context of supersymmetry, searches could be made for scalar electron and chargino pair production[6]. For example, the chargino production process $e^-e^- \rightarrow \chi^- \chi^-$ with $\chi^- \rightarrow W^- \chi^0$ decays gives W^-W^- final states. Searches could also be made for doubly-charged Higgs bosons[7,8,9,10], doubly-charged gauge bosons[11] or W_R production[12]. Massive Majorana neutrino exchange could allow $e^-e^- \rightarrow W^-W^-$ production[13], although due to double β -decay constraints the cross section must be very small. Tests of anomalous vector boson couplings could be made[14], such as the $WW\gamma$ coupling from the $e^-e^- \rightarrow e^-W^-\nu_e$ process.

In the present paper we calculate SM expectations for single and pair production of vector bosons in e^-e^- collisions which are of interest for tests of electroweak theory and as backgrounds to new physics possibilities. We calculate the associated production of a neutral Higgs boson and a weak boson. We also study the possibility of detecting strong W^-W^- scattering and quantitatively evaluate the enhancement of W^-W^- production due to a

doubly-charged Higgs boson. At the end, we will briefly discuss the effects of beamstrahlung and bremsstrahlung on the effective center-of-mass energies and the effective luminosities of the e^-e^- colliders. We also consider the advantages of having both e^- beams polarized.

2. Single weak boson production

Production of weak bosons occurs at order α^3 in the processes

$$e^-e^- \rightarrow e^-W^-\nu_e, \quad (1a)$$

$$e^-e^- \rightarrow e^-Ze^-, \quad (1b)$$

whose Feynman diagrams are given in Fig. 1. The helicity amplitudes can be straightforwardly written down. The resulting total cross sections are shown versus \sqrt{s} in Fig. 2. At $\sqrt{s} = 0.5$ TeV the W^- and Z cross sections are approximately equal and have the value 7 pb; thus with 10 fb^{-1} luminosity about 7×10^4 each of single W and single Z events would be produced at this energy.

In typical accelerator designs the beam hole region is $\theta < 15^\circ$ (or equivalently the beam hole pseudorapidity range is $|\eta| > 2$). We have evaluated the effect of making such an acceptance cut on the leptons (e^-, μ^-) or quark jets from W and Z decays, including the full spin correlations from the weak boson production and decay sequence. With the lepton (quark) decay products of the weak bosons within the $15^\circ < \theta < 165^\circ$ acceptance region the cross sections at $\sqrt{s} = 0.5$ TeV are 1.4 (4.0) pb for W and 0.15 (1.6) pb for Z , including the decay branching fractions.

3. Double weak boson production

Pair production of vector bosons occurs at order α^4 in the processes

$$e^-e^- \rightarrow e^-e^-W^+W^-, \quad (2a)$$

$$e^-e^- \rightarrow e^-\nu_eW^-Z, \quad (2b)$$

$$e^-e^- \rightarrow \nu\nu W^-W^-, \quad (2c)$$

$$e^-e^- \rightarrow e^-\nu_e W^-\gamma \quad (2d)$$

$$e^-e^- \rightarrow e^-e^- ZZ. \quad (2e)$$

The Feynman diagrams for reaction (2c) are shown in Fig. 3.

The analogues of most of these processes at e^+e^- colliders have been calculated in Ref. [15]. The formulas for the e^+e^- amplitudes given in Ref. [15] can be properly crossed to obtain the corresponding amplitudes for e^-e^- collisions. The e^+e^- analogue of the process (2d) was not previously considered but these amplitudes can be obtained by modifying the $e^-e^- \rightarrow e^-\nu_e W^-Z$ amplitudes, changing the Z -couplings to the corresponding γ couplings.

Since the process $e^-e^- \rightarrow e^-\nu_e W^-\gamma$ is essentially the photon-bremsstrahlung contribution to the single W production, we impose acceptance cuts on the final state γ to distinguish it from the single W process. The chosen acceptance cuts are

$$p_{T\gamma} > 10 \text{ GeV}, \quad |\cos\theta_\gamma| < \cos(15^\circ), \quad \theta(\gamma, e_{\text{final}}^-) > 5^\circ, \quad (3)$$

where $\theta(\gamma, e_{\text{final}}^-)$ represents the angle between the photon and the final state electron 3-momenta.

Figure 4 shows the total cross sections for the reactions (2a)–(2e) versus \sqrt{s} for $m_H = 100$ GeV. The value of $m_H = 100$ GeV is taken as representative since the cross section is insensitive to the value of m_H for $m_H \lesssim 2M_W$. The large size of the W^+W^- , $W^-\gamma$, and W^-Z processes is due to photon exchange contributions.

4. Standard-Model Higgs production

In e^+e^- collisions the Standard-Model Higgs boson is produced via $e^+e^- \rightarrow \bar{\nu}_e\nu_e H$ and $e^+e^- \rightarrow ZH$ processes. In e^-e^- collisions single Higgs production can occur via the processes

$$e^-e^- \rightarrow e^-e^- H \quad (4a)$$

$$e^-e^- \rightarrow e^- \nu_e W^- H \quad (4b)$$

$$e^-e^- \rightarrow e^-e^- ZH \quad (4c)$$

The tree-level Feynman diagrams for (4a) and (4b) are shown in Fig. 5. The cross sections are shown in Fig. 6 versus \sqrt{s} for $m_H = 100$ GeV and versus m_H at $\sqrt{s} = 0.5$ TeV; for $m_H = 100$ GeV the $e^-e^- \rightarrow e^-e^-H$ cross section is 9 fb. In comparison to the Higgs production cross section at $\sqrt{s} = 0.5$ TeV in e^+e^- collisions are 60 fb for $Z^* \rightarrow ZH$ and 95 fb for $W^*W^* \rightarrow H$ mechanisms [15]. Higgs production can also occur via $\gamma\gamma$ and γZ fusion at the one-loop level.

For m_H close to M_Z the Z -production processes (1b), (2b), (2e) are large backgrounds to the Higgs processes (4a), (4b), (4c) respectively. For example, for the production of a 100 GeV Higgs boson at $\sqrt{s} = 0.5$ TeV, $\sigma(e^-e^- \rightarrow e^-e^-H) = 9$ fb and $\sigma(e^-e^- \rightarrow e^-e^-Z) = 7000$ fb. The Higgs boson decays dominantly to $b\bar{b}$ while the $Z \rightarrow b\bar{b}$ branching fraction is 0.15. The H -production is central while the Z -production is peaked at forward and backward scattering angles; thus the Z background can be selectively suppressed by angular cuts. In the following we consider the observability of $e^-e^- \rightarrow e^-e^-H$ with $H \rightarrow b\bar{b}$ decays.

The complete $e^-e^- \rightarrow e^-e^-b\bar{b}$ background includes both $e^-e^- \rightarrow e^-e^-Z$ with $Z \rightarrow b\bar{b}$ and the two-photon production of $b\bar{b}$. Based on the fact that the two-photon background can be reduced substantially by keeping the photon propagators far off-shell, we impose the following acceptance cuts

$$p_{Te} > 15 \text{ GeV} \quad \text{and} \quad |\cos \theta_e| < \cos(15^\circ), \quad (5)$$

on both of the electrons in the final state. We also impose the following acceptance cuts on the b 's in the final state:

$$p_{Tb} > 25 \text{ GeV} \quad \text{and} \quad |\cos \theta_b| < 0.7. \quad (6)$$

The latter cuts are tailored to reduce the eeZ background, as the b 's from Z -boson production are much more forward-peaked than the b 's from Higgs-boson production.

Table 1: The Higgs boson signal in the production of $e^-e^- \rightarrow e^-e^-H$ for $m_H = 60\text{--}140$ GeV and the background from $e^-e^- \rightarrow e^-e^-b\bar{b}$ with the invariant mass of the $b\bar{b}$ pair in the range $m_H \pm \Delta m_H$, with $\Delta m_H = 10$ GeV. For simplicity we take $B(H \rightarrow b\bar{b}) = 1$, and assume that all the signal falls within $m_H \pm \Delta m_H$. The acceptance cuts are $p_{Te} > 15$ GeV and $|\cos\theta_e| < \cos(15^\circ)$ on the final state electrons, and $p_{Tb} > 25$ GeV and $|\cos\theta_b| < 0.7$ on the final state b 's.

m_H	Signal (fb)	Background (fb)
60	1.4	0.02
70	1.4	0.03
80	1.4	0.27
90	1.4	1.1
100	1.4	0.86
120	1.3	0.02
140	1.3	0.01

After imposing (5) and (6), the Higgs signal is 1.4 fb for $m_H = 100$ GeV while the total $eeb\bar{b}$ background integrated over all $m(b\bar{b})$ is 1.3 fb. The background has a wide $m(b\bar{b})$ invariant mass distribution (see Fig. 7) with a peak at $m(b\bar{b}) = M_Z$ due to $e^-e^- \rightarrow e^-e^-Z$. The signal is a sharp peak at the Higgs mass. We consider an invariant mass resolution Δm_H for the $b\bar{b}$ pair of 10 GeV and assume that all the signal falls within $m_H \pm \Delta m_H$. The signal and the background in such bins at various Higgs mass values are summarized in Table 1. In this simple comparison we have assumed perfect b -tagging with only the $b\bar{b}$ final state counted as background, *i.e.*, the other $q\bar{q}$ ($q = u, d, s, c$) final states are rejected. The background for $m_H = 90$ GeV is the largest because of $ee \rightarrow eeZ$. We conclude that the intermediate mass Higgs boson in the channel $e^-e^- \rightarrow e^-e^-H$ with $H \rightarrow b\bar{b}$ may be observable with an integrated luminosity of at least 20 fb^{-1} .

When $m_H > 2m_Z$, Higgs production with $H \rightarrow ZZ$ decay can give an appreciable enhancement to the $e^-e^- \rightarrow e^-e^-ZZ$ production; for example, at $m_H = 200$ GeV the cross

section of $e^-e^- \rightarrow e^-e^-ZZ$ is a factor of two larger than that with $m_H = 100$ GeV.

5. Strong W_LW_L Scattering

If no light Higgs boson is found for $m_H \lesssim 800$ GeV, one would anticipate that the interactions among longitudinal vector bosons become strong[16]. An e^-e^- collider offers a unique opportunity to explore the weak isospin $I = 2$ s -channel [17] via the process $W_L^-W_L^- \rightarrow W_L^-W_L^-$ [18]. The simplest model for a strongly-interacting $W_L^-W_L^-$ sector is the exchange of a heavy Higgs boson. This results in an enhancement of the $e^-e^- \rightarrow \nu\nu W^-W^-$ production cross section compared to that expected from the exchange of a light Higgs boson. This enhancement due to a Higgs boson of mass 1 TeV can be defined as the difference of the $W_L^-W_L^- \rightarrow W_L^-W_L^-$ fusion contributions

$$\Delta\sigma_H = \sigma(m_H = 1 \text{ TeV}) - \sigma(m_H = 0.1 \text{ TeV}) \quad (7)$$

to $e^-e^- \rightarrow \nu\nu W^-W^-$ production. There is no appreciable numerical change between the choices $m_H = 0.1$ TeV and $m_H = 0$ for the light Higgs boson reference mass. We find the values

$$\Delta\sigma_H \simeq \begin{cases} 53.6 - 50.9 = 2.7 \text{ fb} & \text{at } \sqrt{s} = 1.5 \text{ TeV}; \\ 86.5 - 82.0 = 4.5 \text{ fb} & \text{at } \sqrt{s} = 2 \text{ TeV}. \end{cases} \quad (8)$$

In the following we address the observability of this strong $W_L^-W_L^- \rightarrow W_L^-W_L^-$ signal at $\sqrt{s} = 2$ TeV. The complete Standard-Model cross section for $e^-e^- \rightarrow \nu\nu W^-W^-$ from all diagrams in Fig. 3 is about 20 times larger than $\Delta\sigma$. Hence the background contributions associated with transverse W bosons ($W_T^-W_T^-$, $W_T^-W_L^-$) must somehow be selectively reduced by acceptance criteria if we are to observe the strongly-interacting $W_L^-W_L^-$ signal.

There are several different ways to accomplish the substantial background suppression[18,19,20]. The $W_L^-W_L^-$ scattering process gives large $M(W^-W^-)$ of order 1 TeV with centrally-produced W^- having large p_T . Thus we impose the kinematic cuts

$$p_T(W) > 150 \text{ GeV}, \quad |\cos\theta_W| < 0.8, \quad (9)$$

which retains about one-third of the signal and reduces the SM backgrounds by more than an order of magnitude. After those cuts, the heavy Higgs enhancement becomes $\Delta\sigma_H \simeq 7.8 - 6.3 = 1.5$ fb.

In hadronic W -decays, the sign of the W charge is not identified and the two-photon process $e^-e^- \rightarrow e^-e^-W^+W^-$ may also present a substantial background when the final electrons are not observed. From Fig. 4 the cross section for $e^-e^- \rightarrow e^-e^-W^+W^-$ is about a factor of 30 larger than $e^-e^- \rightarrow \nu\nu W^-W^-$. Moreover, $e^-e^- \rightarrow e^-\nu W^-Z$ could add to the background if the reconstructed invariant masses in hadronic decays are not sufficiently resolved to distinguish W from Z . In order to suppress these backgrounds we veto events in which an electron can be identified having[21]

$$E_e > 50 \text{ GeV}, \quad |\cos\theta_e| < |\cos(150 \text{ mrad})|. \quad (10)$$

With the acceptance of Eqs. (9) and (10), the remaining $e^-e^- \rightarrow e^-e^-W^+W^-$ and $e^-e^- \rightarrow e^-\nu_e W^-Z$ backgrounds are 60 fb and 10 fb, respectively.

A further improvement in isolating the $W_L^-W_L^-$ signal derives from the fact that the $p_T(WW)$ spectrum of the signal is peaked around M_W and falls off rapidly at high p_T like $1/p_T^4$. Figure 8(a) compares the $p_T(VV)$ distribution of the $W_L^-W_L^-$ signal with the backgrounds. Note that the difference between the solid curve (with $m_H = 1$ TeV) and the dashed curve (with $m_H = 0.1$ TeV) is the strong $W_L^-W_L^-$ enhancement. We impose the selection

$$50 \text{ GeV} < p_T(VV) < 300 \text{ GeV} \quad (11)$$

for additional background suppression.

The signal gives W_L^- bosons that are fast and moving back-to-back in the transverse plane. The difference in the transverse momenta of the two weak bosons is

$$\Delta p_T(VV) = |\mathbf{p}_T(V_1) - \mathbf{p}_T(V_2)| \quad (12)$$

presented in Fig. 8(b). The signal (difference of solid and dashed curves) is enhanced by the

cut

$$\Delta p_T(VV) > 400 \text{ GeV}. \quad (13)$$

With the additional cuts of Eqs. (11) and (13) the surviving signal is

$$\Delta\sigma_H \simeq 3.8 - 2.8 = 1.0 \text{ fb}. \quad (14)$$

The efficiency for retaining the signal is 67%. The remaining backgrounds are 4.4 fb for $e^-e^- \rightarrow e^-e^-W^-W^+$ and 4.7 fb for $e^-e^- \rightarrow e^-\nu W^-Z$. The resulting $M(VV)$ distributions after these cuts are presented in Fig. 9. At high VV invariant masses the strong $W_L^-W_L^-$ scattering rate due to the exchange of a 1 TeV Higgs boson is enhanced over the $W_T^-W_T^-$, $W_T^-W_L^-$ and W^-W^+ backgrounds, while the background due to W^-Z still persists.

Next we estimate the signal rates for other strongly-interacting scenarios. We consider a chirally-coupled scalar boson ($m_S = 1 \text{ TeV}$ and $\Gamma_S = 350 \text{ GeV}$), a chirally-coupled vector boson ($m_V = 1 \text{ TeV}$ and $\Gamma_V = 25 \text{ GeV}$)[18,19], and the low energy theorem amplitude[19,22]. These calculations are carried out with the effective W -boson approximation (EWA) [23]. In this calculational method one is unable to obtain the exact kinematics for the final state of W^-W^- . In order to simulate the acceptance effects of Eqs. (11) and (13), we multiplied the EWA calculations by the efficiency factor 67% found in the heavy Higgs boson model.

The predicted cross sections at $\sqrt{s} = 2 \text{ TeV}$ with the cuts discussed above are presented in Table 2. Also given in parentheses are the number of events with hadronic W, Z decays for an integrated luminosity of 300 fb^{-1} . In Table 2 we see that the backgrounds (dominantly from W^-Z production) to the signals are still substantial after the kinematic selection criteria. Due to the absence of an s -channel resonance, the signals are mostly an overall enhancement on the M_{WW} spectrum. If we can predict the SM backgrounds at a level of better than 10%, there is a chance that we can observe the strong W^-W^- scattering via the hadronic decay modes at statistical significance $S/\sqrt{B} > 4$ for a 1 TeV scalar or a vector particle, and at $S/\sqrt{B} \geq 6.4$ for the LET amplitude with $M_{WW} > 500 \text{ GeV}$.

If separation of W and Z peaks can be achieved in the m_{jj} mass distributions then the

Table 2: Cross sections at $\sqrt{s} = 2$ TeV from different models of strongly-interacting W^-W^- with cuts discussed in the text. Backgrounds are summed over W^-W^- with a light Higgs exchange, W^+W^- , and W^-Z . Entries are in units of fb and those in parentheses correspond to the number of events with hadronic W, Z decays for an integrated luminosity of 300 fb^{-1} .

M_{WW}^{min}	SM $m_H = 1 \text{ TeV}$	Scalar $m_S = 1 \text{ TeV}$	Vector $m_V = 1 \text{ TeV}$	LET	Backgrounds
0.5 TeV	0.88 (130)	1.2 (175)	1.1 (167)	1.7 (245)	10 (1470)
0.75 TeV	0.44 (65)	0.72 (106)	0.63 (93)	1.0 (150)	3.5 (515)
1 TeV	0.15 (22)	0.31 (46)	0.26 (38)	0.48 (71)	1.0 (147)

backgrounds would be significantly further reduced. The use of $Z \rightarrow e^+e^-, \mu^+\mu^-, b\bar{b}$ (with b -tagging), with combined branching fraction of about 22%, could be helpful in determining the contribution of the W^-Z process.

6. H^{--} Signal in Scalar Doublet + Triplet Model

The charged Higgs boson in SUSY and other two-Higgs-doublet models can be pair-produced [24] via $e^-e^- \rightarrow \nu\nu H^-H^-$ via the W^-W^- fusion subprocess with H^0 exchange; see Fig. 10(a). If the H^- is not degenerate in mass with W , this H^-H^- signal could be spectacular and sensitive to the model parameters, such as the ratio of vacuum expectation values $\tan\beta = v_2/v_1$.

A search for a doubly-charged Higgs boson in a model with a scalar triplet could also be carried out at an e^-e^- collider. What makes the e^-e^- collider unique in this instance is that the doubly-charged Higgs boson can be produced as an s -channel resonance via $W^-W^- \rightarrow H^{--}$ [see Fig. 10(b)], followed by $H^{--} \rightarrow W^-W^-, W^-H^-$ and possibly $f\bar{f}'$ decays [9], depending on the model parameters. Detailed analyses of the doublet plus triplet model can be found in the literature[9] and we will not repeat the discussion of the model here. The model contains an SU(2) five-plet $H_5^{+,+,0,-,-}$, a triplet $H_3^{+,0,-}$, and 2 singlets H_1^0 and H_1^{\prime} . For simplicity, we assume that in the Higgs potential[9] that there is no mixing

between the singlets (therefore $\lambda_3 = 0$) and that all other λ -couplings are of similar size ($\lambda_1 \simeq \lambda_2 \simeq \lambda_4 \simeq \lambda_5$). There are then two independent parameters left in the model: the mass parameter of the five-plet, m_5 , and the mixing angle θ_H between the Higgs doublet and the triplet fields, which is related to the ratio of the vacuum expectation values. Figure 11 presents the $M_{W^-W^-}$ distribution at $\sqrt{s} = 0.5$ TeV including the resonance process $e^-e^- \rightarrow \nu\nu H^{--} \rightarrow \nu\nu W^-W^-$ with $m_5 = M(H^{--}) = 0.2$ or 0.3 GeV, taking maximum mixing $\tan\theta_H = 1$. A significant enhancement above the SM background occurs.

7. Beamstrahlung Effects

Since beamstrahlung is a collective phenomenon, it depends very much on the design of the machine, *e.g.*, the number of particles in a bunch, the number of bunches in the beam, and the shape of the beam. Systematic studies of beamstrahlung at e^+e^- colliders have been made; see Ref. [25]. Based on these analyses we briefly comment on beamstrahlung effects on the luminosity and the center-of-mass energy of an e^-e^- collider.

In e^+e^- collisions, the forces on the charged particles in one of the beams due to the electromagnetic field of the opposite beam cause the particles to curve towards the center of the beam, resulting in a more compact beam and so the effective luminosity increases. For example, in the NLC design[3] the luminosity enhancement factor H_D is 1.4, while that for the DLC design[3] is 2.8. The effect of beamstrahlung on the luminosities in e^-e^- collisions is exactly opposite, due to the fact that the force from the opposite beam causes the particle to diverge from the center of the beam. The decrease in the luminosity of the e^-e^- colliders (assuming the same design as the corresponding e^+e^- colliders) is a factor of 0.7 for the NLC design and 0.36 for the DLC design. However, the luminosity decreases can likely be reduced by the altering the designs. Bremsstrahlung does not change the luminosity.

The effect of beamstrahlung on the center-of-mass energy \sqrt{s} is easy to understand. The forces felt by one of the beams due to the fields of the opposite beam in either e^+e^- or e^-e^- collisions are equal, though in opposite directions. The accelerations of the charged particles

in the beam are therefore equal for e^+e^- and e^-e^- collisions (again in opposite directions), and so the radiations from the accelerated charges are the same. Thus, the resultant decreases in the center-of-mass energies due to radiation are the same for e^+e^- and e^-e^- colliders. In the DLC, NLC, JLC, and TESLA designs[3] the decreases in the center-of-mass energies due to beamstrahlung effects can be controlled better than that of bremsstrahlung, which is well understood. Since the cross sections of all the processes considered in this paper increase with \sqrt{s} , the decrease in the effective center-of-mass energy due to beamstrahlung and bremsstrahlung will decrease the cross sections.

8. Advantages of Polarizing the Electron Beams

There are advantages of polarizing the colliding electron beams either left-handed or right-handed. Only the left-handed fermions ($e_L^-, \nu_L, u_L, d_L, \dots$) and the right-handed anti-fermions ($e_R^+, \bar{\nu}_R, \bar{u}_R, \bar{d}_R, \dots$) couple to the SM W boson. By the use of polarized electrons the backgrounds can be reduced according to the nature of the signals of interest. For example, to search for the right-handed W boson that exists in left-right models, it will be advantageous to use e_R^- beams in order to reduce the SM W production. By colliding e_L^- beams the strong $W_L^-W_L^-$ signal in the process $e^-e^- \rightarrow \nu_e\nu_e W_L^-W_L^-$ (where W_L denotes longitudinal polarization) can be enhanced over the W^+W^- , ZZ , and W^-Z backgrounds. Similarly, the signals of H^{--} and H^-H^- will be favored with the use of e_L^- beams. In Table 3 we compare the relative sizes of the polarized cross sections for the SM processes that we have calculated in this paper. There are four possible polarization combinations (LL, LR, RL, and RR). We denote, *e.g.*, σ_{LL} as the cross section if both of the incoming electrons are left-handed.

9. Summary

We have calculated the Standard-Model cross sections for single and double production of weak bosons, which are SM backgrounds in the search for new physics in high energy e^-e^-

Table 3: A comparison of the cross sections of SM processes for different polarizations (LL, LR, RL, and RR) of the incoming electrons.

Process $e^-e^- \rightarrow$	Relation among the σ 's
$e^-\nu_e W^-$	$\sigma_{LL} > \sigma_{LR} = \sigma_{RL} > \sigma_{RR} = 0$
$e^-e^- Z$	$\sigma_{LL} > \sigma_{LR} = \sigma_{RL} > \sigma_{RR}$
$e^-e^- W^+W^-$	$\sigma_{LL} > \sigma_{LR} = \sigma_{RL} > \sigma_{RR}$
$e^-\nu_e W^-Z$	$\sigma_{LL} > \sigma_{LR} = \sigma_{RL} > \sigma_{RR} = 0$
$\nu_e\nu_e W^-W^-$	$\sigma_{LL} > \sigma_{LR} = \sigma_{RL} = \sigma_{RR} = 0$
$e^-\nu_e W^-\gamma$	$\sigma_{LL} > \sigma_{LR} = \sigma_{RL} > \sigma_{RR} = 0$
$e^-e^- ZZ$	$\sigma_{LL} > \sigma_{LR} = \sigma_{RL} > \sigma_{RR}$
$e^-e^- H$	$\sigma_{LL} > \sigma_{LR} = \sigma_{RL} > \sigma_{RR}$
$e^-\nu_e W^-H$	$\sigma_{LL} > \sigma_{LR} = \sigma_{RL} > \sigma_{RR} = 0$
$e^-e^- ZH$	$\sigma_{LL} > \sigma_{LR} = \sigma_{RL} > \sigma_{RR}$

collisions. Single and associated Higgs boson productions have also been calculated and can give observable signals, although the cross sections are generally not as large as those in e^+e^- collisions. We have also investigated the possibility of observing strong $W_L^-W_L^-$ scattering, which occurs through the weak isospin $I = 2$ channel and is unique to e^-e^- collisions. We have developed certain kinematic cuts to significantly reduce the $W_T^-W_T^-$, $W_T^-W_L^-$, W^+W^- and W^-Z backgrounds to the strong $W_L^-W_L^-$ signal in hadronic decay modes. The W^-Z background persists at large M_{WW} , which makes the observation of strong $W_L^-W_L^-$ scattering difficult. On the other hand, if doubly-charged Higgs bosons exist, the s -channel enhancement in W^-W^- final state would be very substantial at an e^-e^- collider. This survey of cross sections and processes should provide useful benchmarks for serious studies of the potential of such a machine for new physics discovery.

Acknowledgments

We thank Pisin Chen for an informative discussion on the subject of beamstrahlung. We also thank David Burke, Clemens Heusch, and Richard Prepost for discussions. This research was supported in part by the U.S. Department of Energy under Contract No. DE-AC02-76ER00881 and in part by the University of Wisconsin Research Committee with funds granted by the Wisconsin Alumni Research Foundation. J.F.B. is supported by a National Science Foundation Graduate Research Fellowship. K.C. is supported by the U.S. D.O.E. grant No. DE-FG02-91ER40684. T.H. is supported in part by the U.S. D.O.E. grant No. DE-FG03-91ER40674, and in part by a UC-Davis Faculty Research Grant.

References

- [1] See *e.g.*, the LEP Collaborations: ALEPH, DELPHI, L3 and OPAL, Phys. Lett. **B276**, 247 (1992); SLD Collaboration, Mod. Phys. Lett. **A8**, 2237 (1993).
- [2] See *e.g.*, K. Riles, in *Proceedings of the Workshop on Physics at Current Accelerators and Supercolliders*, Argonne, Illinois (June 1993), ed. J.L. Hewett *et al.* (ANL-HEP-CP-93-92, 1993), p. 103.
- [3] *Proceedings of the Workshop on Physics and Experiments with Linear e^+e^- Colliders*, Waikoloa, Hawaii (April 1993), ed. F. Harris *et al.* (World Scientific, 1993); JLC Group, KEK Report 92-16 (1992); *Proceedings of the Workshop on Physics and Experiments with Linear Colliders*, Saariselkä, Finland (Sept. 1991), ed. R. Orava *et al.* (World Scientific, 1992).
- [4] See *e.g.*, *Proceedings of the SLC Workshop on Experimental Use of the SLAC Collider*, Stanford, California (Dec. 1981), SLAC-247 (1982), p. 606.
- [5] C. Heusch, in *Proceedings of the Workshop on Physics and Experiments with Linear e^+e^- Colliders*, Waikoloa, Hawaii (April 1993), ed. F. Harris *et al.* (World Scientific, 1993), pp. 895, 917; J.F. Gunion, *ibid.*, p. 903; P.H. Frampton, *ibid.*, p. 911; J. Blümlein and P.H. Frampton, *ibid.*, p. 926.
- [6] F. Cuypers, G.J. van Oldenborgh, and R. Rückl, CERN-TH.6740/92 (1992); Nucl. Phys. **B409**, 128 (1993); MPI-PH-93-70 (1993).
- [7] H. Georgi and M. Machacek, Nucl. Phys. **B262**, 463 (1985).
- [8] D.A. Dicus and R. Vega, Nucl. Phys. **B329**, 553 (1990).
- [9] J.F. Gunion, R. Vega, and J. Wudka, Phys. Rev. **D42**, 1673 (1990); J.F. Gunion, in Ref. [5].

- [10] R.S. Chivukula and H. Georgi, Phys. Lett. **B182**, 181 (1986).
- [11] P. Frampton, Phys. Rev. Lett. **69**, 2889 (1992); F. Pisano and V. Pleitez, Phys. Rev. **D46**, 410 (1992); P. Frampton, in Ref. [5].
- [12] T.G. Rizzo, SLAC-PUB-6475 (1994).
- [13] T.G. Rizzo, Phys. Lett. **B116**, 23 (1982); C.A. Heusch and P. Minkowski, CERN-TH.6606-92 (1993).
- [14] D. Choudhury and F. Cuypers, MPI-Ph/93-98 (1993).
- [15] V. Barger, Kingman Cheung, B.A. Kniehl, and R.N.J. Phillips, Phys. Rev. **D46**, 3725 (1992).
- [16] M.S. Chanowitz and M.K. Gaillard, Nucl. Phys. **B261**, 379 (1985).
- [17] M. S. Chanowitz and M. Golden, Phys. Rev. Lett. **61**, 1053 (1988); **63**, 466(E) (1989); V. Barger, K. Cheung, T. Han, and R.J.N. Phillips, Phys. Rev. **D42**, 3052 (1990); D. Dicus, J.F. Gunion, and R. Vega, Phys. Lett. **258B**, 475 (1991); M. S. Berger and M. S. Chanowitz, Phys. Lett. **263B**, 509 (1991); M.S. Chanowitz and W. Kilgore, Phys. Lett. **B322**, 147 (1994).
- [18] T. Han, in *Proceedings of the Workshop on Physics and Experiments with Linear e^+e^- Colliders*, Waikoloa, Hawaii (April 1993), ed. F. Harris *et al.* (World Scientific, 1993), p. 270.
- [19] J. Bagger, V. Barger, K. Cheung, J. Gunion, T. Han, G. Ladinsky, R. Rosenfeld and C.P. Yuan, Phys. Rev. **D49**, 1246 (1994).
- [20] K. Cheung, in *Proceedings of the Workshop on Physics and Experiments with Linear e^+e^- Colliders*, Waikoloa, Hawaii (April 1993), ed. F. Harris *et al.* (World Scientific, 1993), p. 864; in *Proceedings of the Workshop on Physics at Current Accelerators and*

Supercolliders, Argonne, Illinois (June 1993), ed. J.L. Hewett *et al.* (ANL-HEP-CP-93-92, 1993), p. 421.

- [21] K. Hagiwara, J. Kanzaki, and H. Murayama, DTP/91/18 (1991).
- [22] S. Weinberg, Phys. Rev. Lett. **17**, 616 (1966); M. S. Chanowitz, M. Golden, and H. Georgi, Phys. Rev. Lett. **57**, 2344 (1986); Phys. Rev. **D35**, 1490 (1987).
- [23] M. S. Chanowitz and M. K. Gaillard, Phys. Lett. **B142**, 85 (1984); G. L. Kane, W. W. Repko and W. R. Rolnick, Phys. Lett. **B148**, 367 (1984); S. Dawson, Nucl. Phys. **B249**, 42 (1985).
- [24] T.G. Rizzo, Phys. Lett. **B244**, 532 (1990).
- [25] P. Chen, Phys. Rev. **D46**, 1186 (1992); in *Proceedings of the Workshop on Physics and Experiments with Linear e^+e^- Colliders*, Waikoloa, Hawaii (April 1993), ed. F. Harris *et al.* (World Scientific, 1993), p. 590; T. Barklow, P. Chen and W. Kozenicki, in *Proceedings of the Workshop on e^+e^- Colliders at 500 GeV: The Physics Potential*, Munich-Annecy-Hamburg (1991), ed. P.M. Zerwas (DESY-92-123, 1992), p. 845.

Figure Captions

1. Representative Feynman diagrams for single W or Z production in e^-e^- collisions. In the case of Z production, diagrams with the interchange of final-state electrons must also be included.
2. Total cross sections for single weak boson production in e^-e^- collisions versus the CM energy \sqrt{s} .
3. Representative Feynman diagrams for W^-W^- production in e^-e^- collisions. Diagrams with the interchange of identical final-state particles (ν 's and W^- 's) must also be included, omitting the interchange of $W^-(k_1)$ and $W^-(k_2)$ in diagram (c).
4. Total cross sections for vector boson pair production (W^-W^+ , $W^-\gamma$, W^-Z , W^-W^- , ZZ) in e^-e^- collisions versus the CM energy \sqrt{s} . The photon in the $W^-\gamma$ case has the acceptance in Eq. (3). The value $m_H = 100$ GeV is assumed.
5. Representative Feynman diagrams for the production of the Standard-Model Higgs boson in e^-e^- collisions. The other diagrams can be obtained by the interchange $p_1 \leftrightarrow p_2$.
6. Cross sections for production of the Standard-Model Higgs boson in e^-e^- collisions (a) versus \sqrt{s} at $m_H = 100$ GeV, (b) versus m_H at $\sqrt{s} = 0.5$ TeV.
7. The differential cross section $d\sigma/dm(b\bar{b})$ versus the invariant mass $m(b\bar{b})$ of the $b\bar{b}$ pair in the process $e^-e^- \rightarrow e^-e^-b\bar{b}$ at $\sqrt{s} = 0.5$ TeV, with the acceptance cuts of Eqs. (5) and (6). The peak at $m(b\bar{b}) \approx M_Z$ is due to $e^-e^- \rightarrow e^-e^-Z$ with $Z \rightarrow b\bar{b}$. The signal due to a Higgs boson of mass $m_H = 120$ GeV is illustrated.
8. Distributions at $\sqrt{s} = 2$ TeV in the transverse momenta of vector bosons produced in the reactions $e^-e^- \rightarrow \nu\nu W^-W^-$, $e^-e^-W^+W^-$, $e^-\nu W^-Z$: (a) $p_T(VV) = |\mathbf{p}_T(V_1) + \mathbf{p}_T(V_2)|$, (b) $\Delta p_T(VV) = |\mathbf{p}_T(V_1) - \mathbf{p}_T(V_2)|$.

9. Invariant mass distributions of the weak boson pairs produced in the reactions $e^-e^- \rightarrow \nu\nu W^-W^-$, $e^-e^-W^+W^-$, $e^-\nu W^-Z$ after the acceptance cuts of Eqs. (11) and (13) have been applied to enhance the strongly-interacting W^-W^- signal due to the exchange of a 1 TeV SM Higgs boson.

10. Representative Feynman diagrams for the production of H^- and H^{--} in e^-e^- collisions. Diagrams with the interchange of identical final-state particles (ν 's and H^- 's) must also be included.

11. The distribution in the W^-W^- invariant mass for $e^-e^- \rightarrow \nu_e\nu_e W^-W^-$ including the contribution of a doubly-charged Higgs boson of mass $M(H^{--}) = 0.2$ or 0.3 TeV.

This figure "fig1-1.png" is available in "png" format from:

<http://arxiv.org/ps/hep-ph/9404335v1>

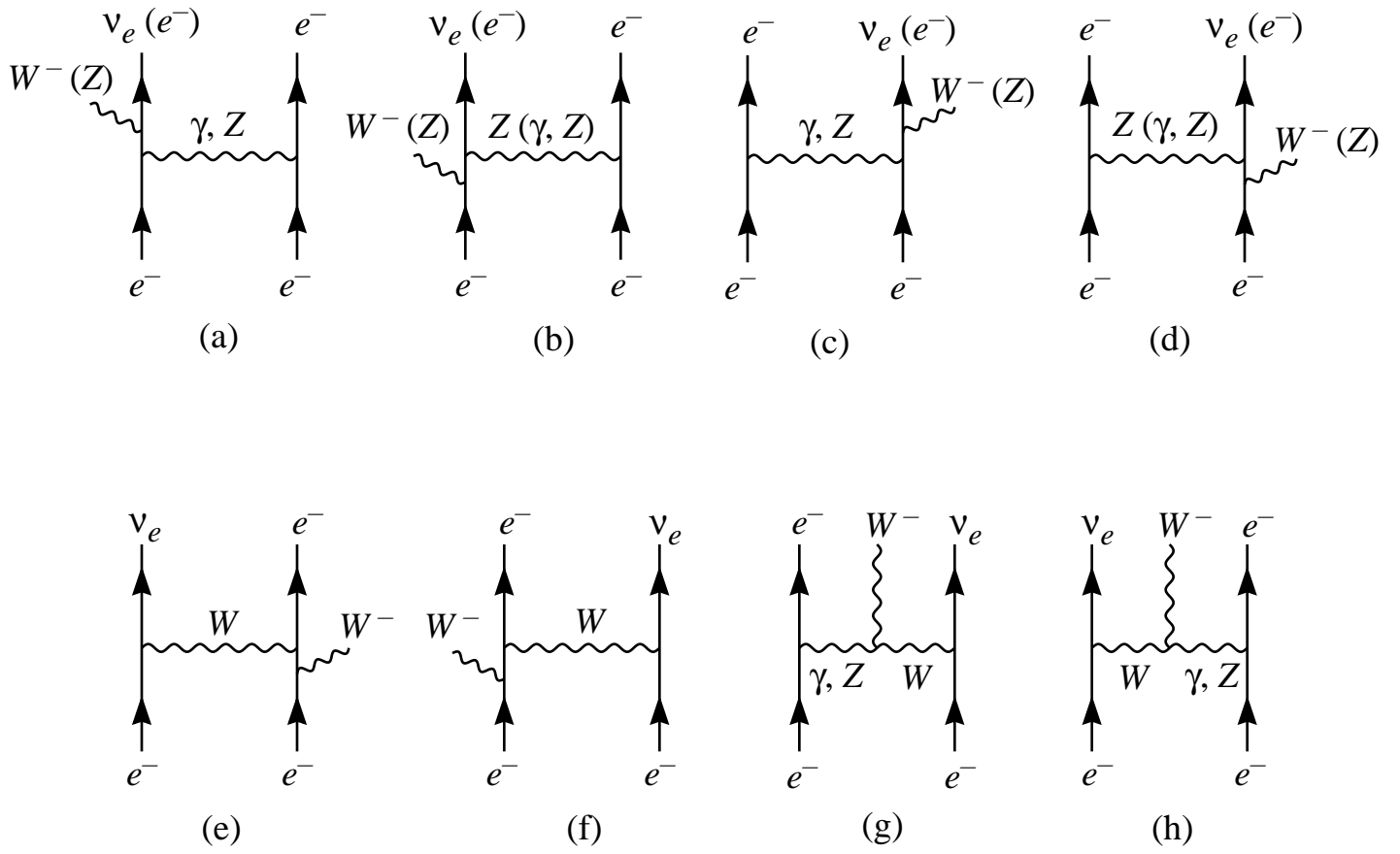


Fig. 1

This figure "fig2-1.png" is available in "png" format from:

<http://arxiv.org/ps/hep-ph/9404335v1>

This figure "fig3-1.png" is available in "png" format from:

<http://arxiv.org/ps/hep-ph/9404335v1>

This figure "fig1-2.png" is available in "png" format from:

<http://arxiv.org/ps/hep-ph/9404335v1>

This figure "fig2-2.png" is available in "png" format from:

<http://arxiv.org/ps/hep-ph/9404335v1>

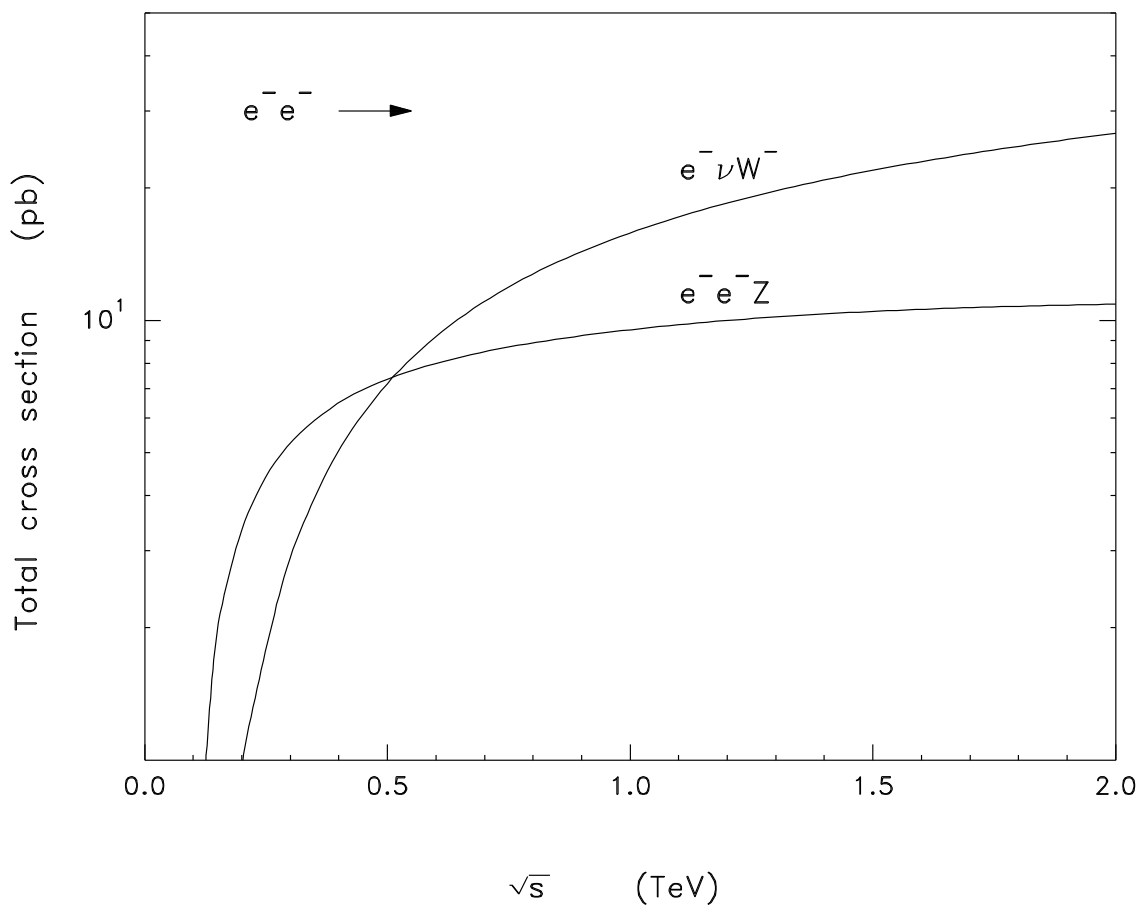


Fig. 2

This figure "fig3-2.png" is available in "png" format from:

<http://arxiv.org/ps/hep-ph/9404335v1>

This figure "fig1-3.png" is available in "png" format from:

<http://arxiv.org/ps/hep-ph/9404335v1>

This figure "fig2-3.png" is available in "png" format from:

<http://arxiv.org/ps/hep-ph/9404335v1>

This figure "fig3-3.png" is available in "png" format from:

<http://arxiv.org/ps/hep-ph/9404335v1>

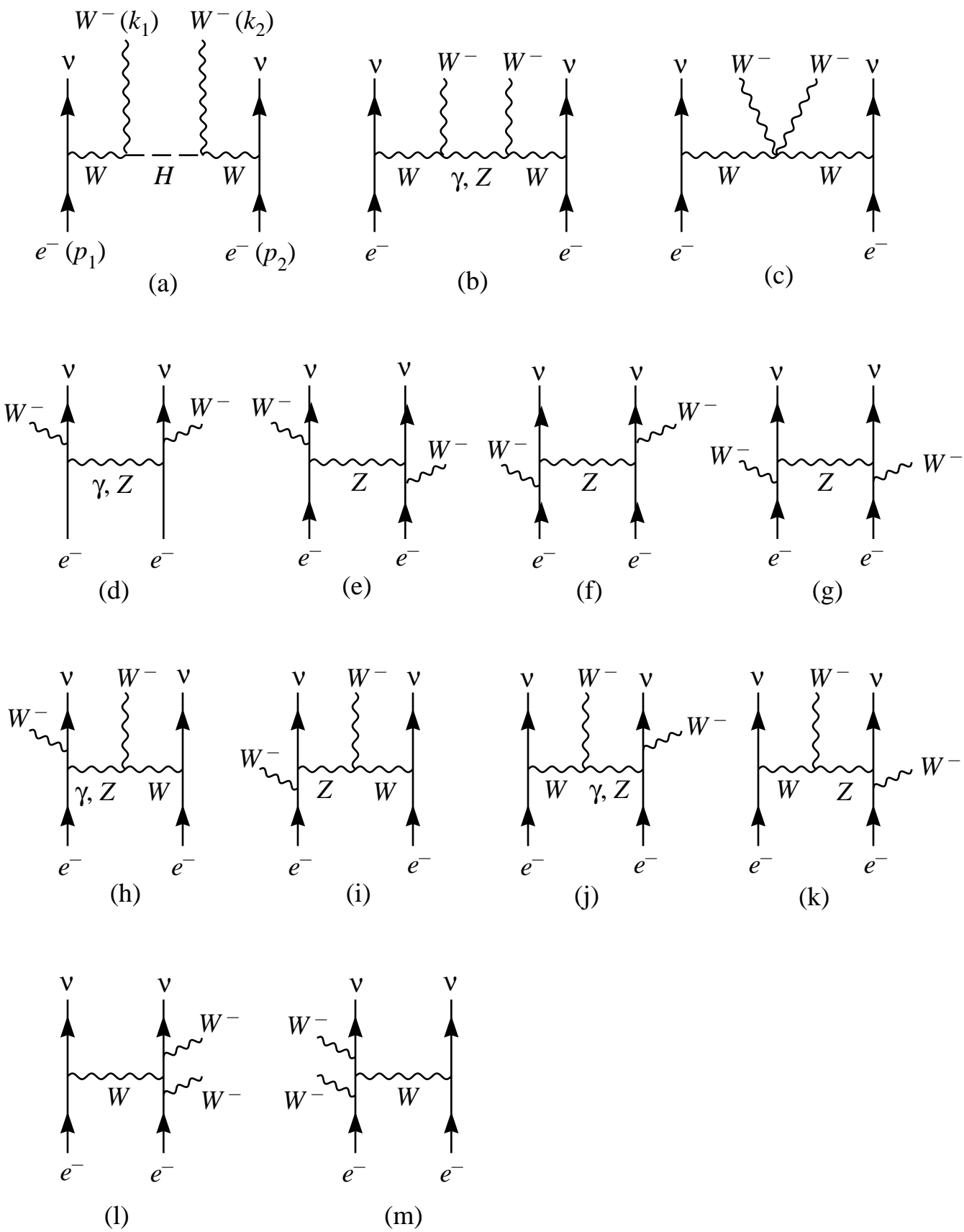


Fig. 3

This figure "fig1-4.png" is available in "png" format from:

<http://arxiv.org/ps/hep-ph/9404335v1>

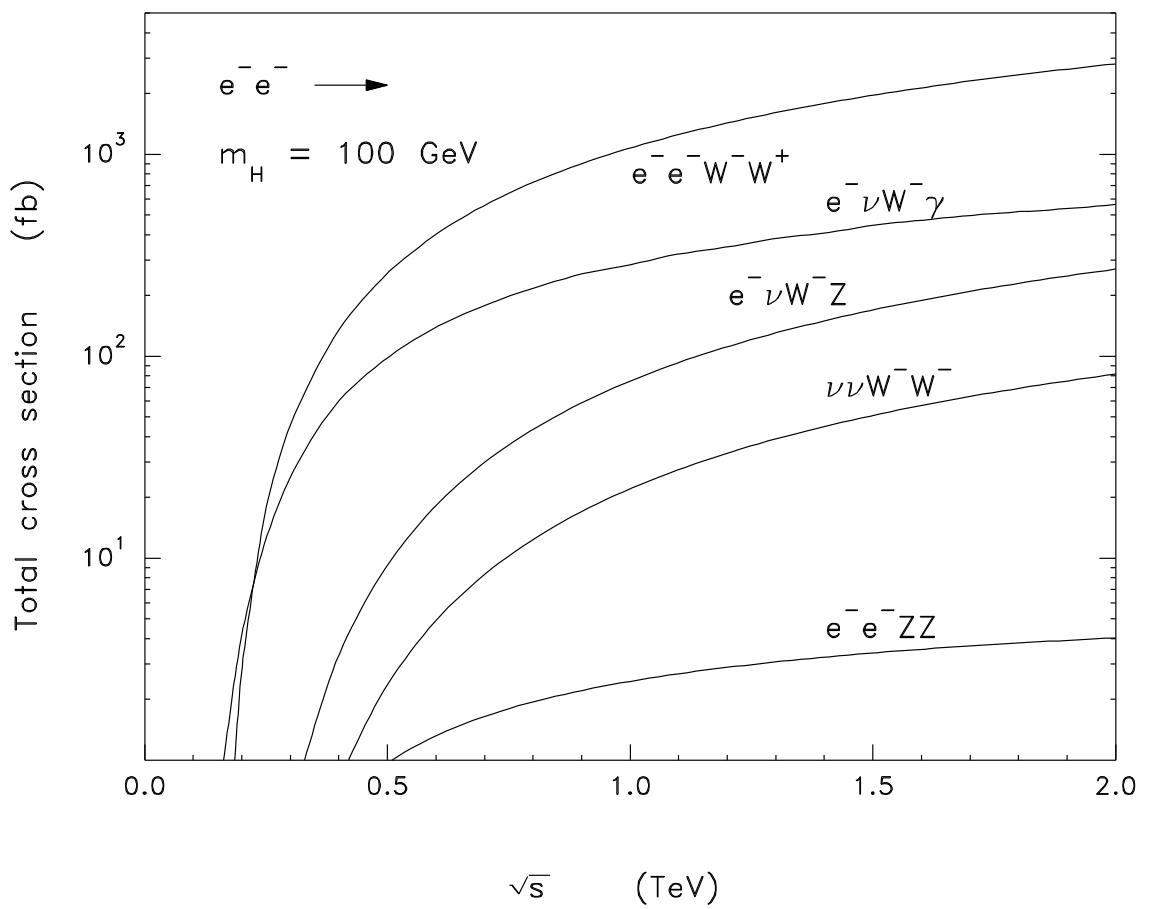


Fig. 4

This figure "fig1-5.png" is available in "png" format from:

<http://arxiv.org/ps/hep-ph/9404335v1>

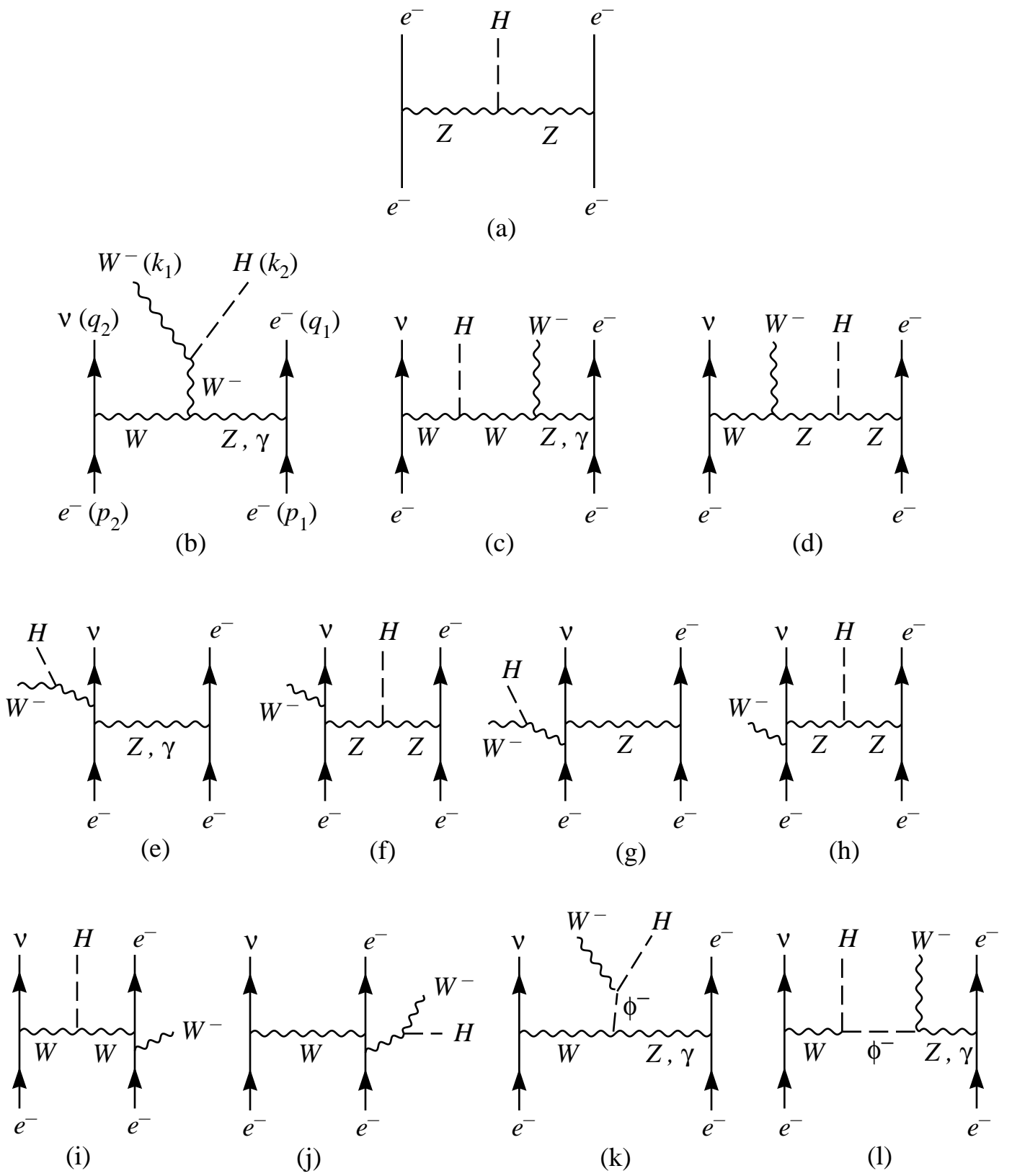


Fig. 5

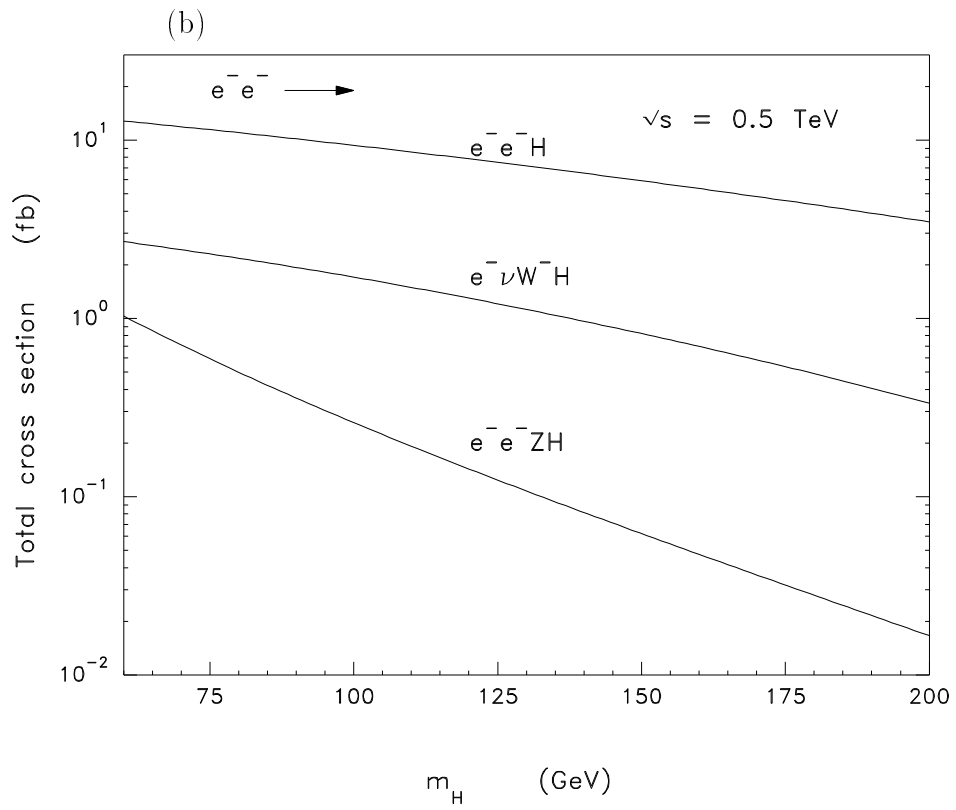
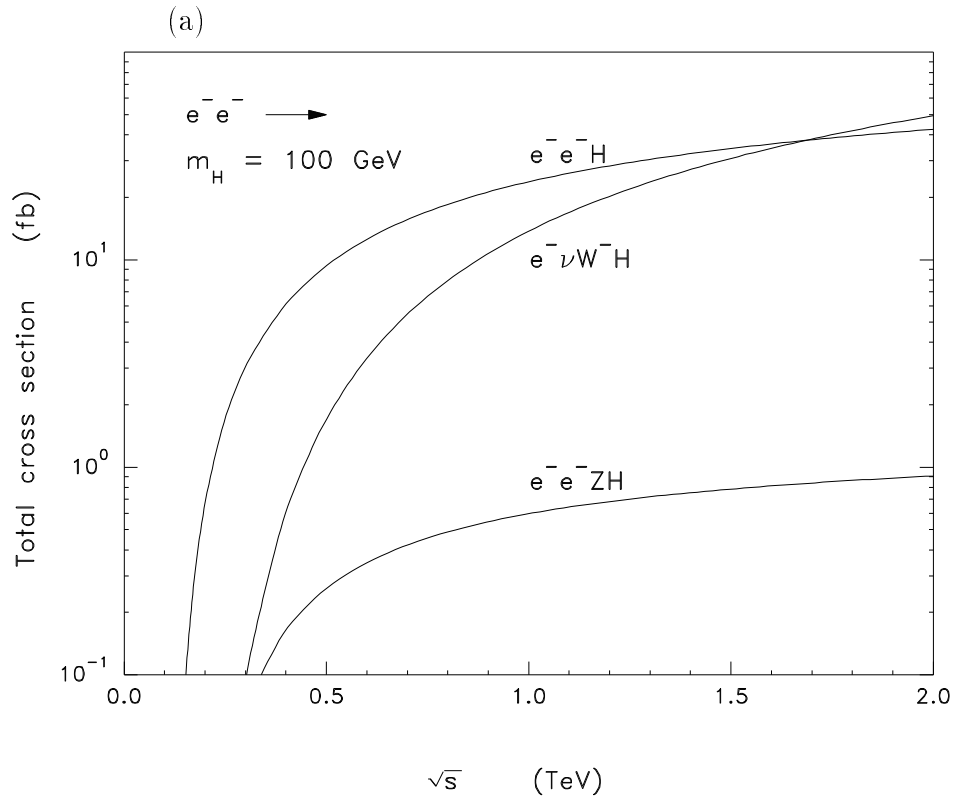


Fig. 6

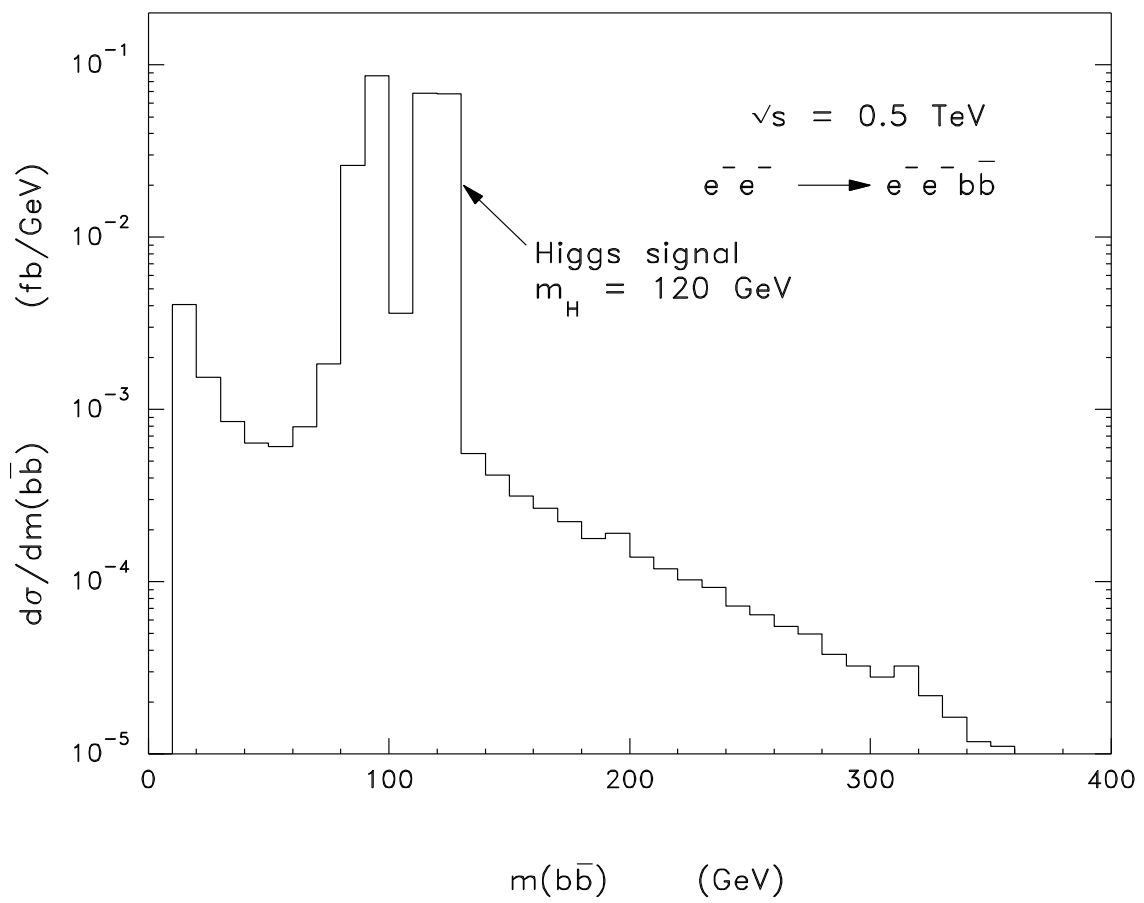


Fig. 7

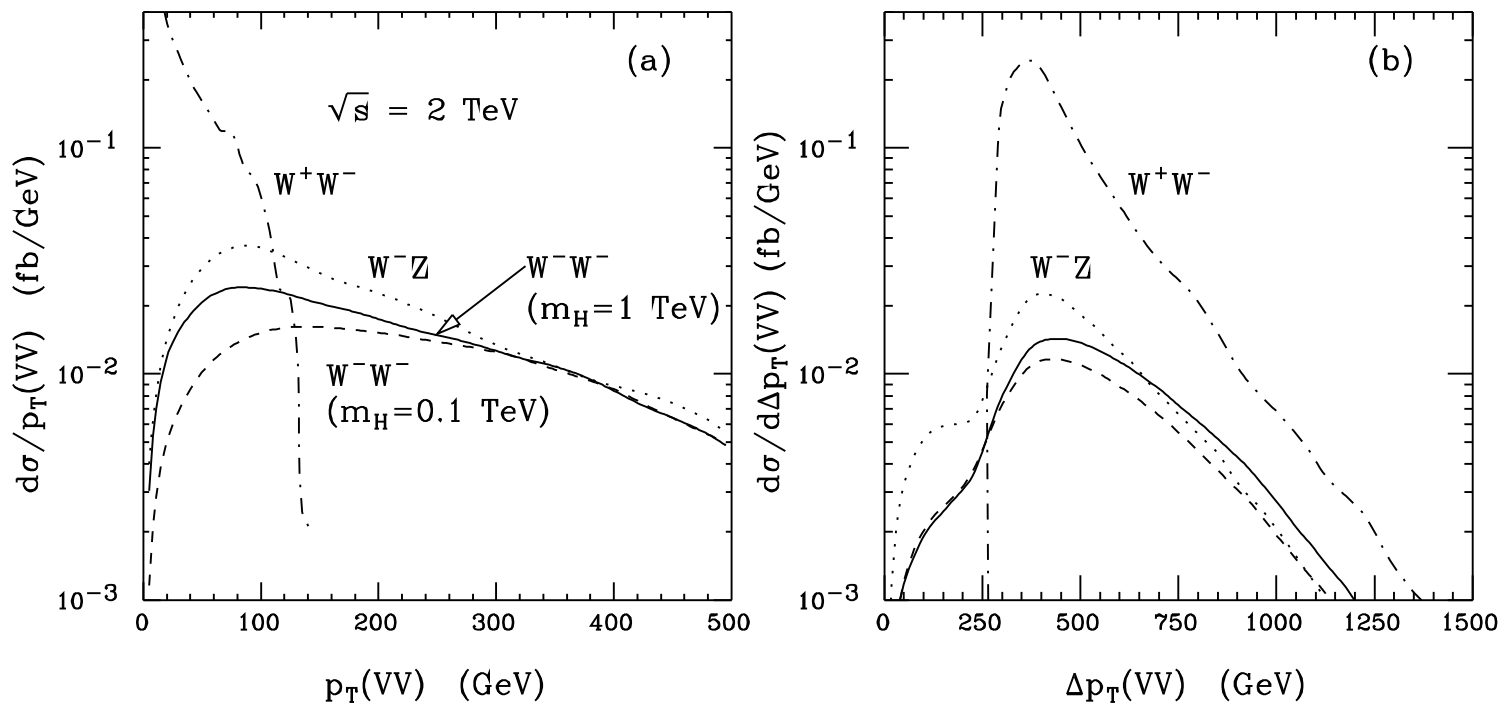


Fig. 8

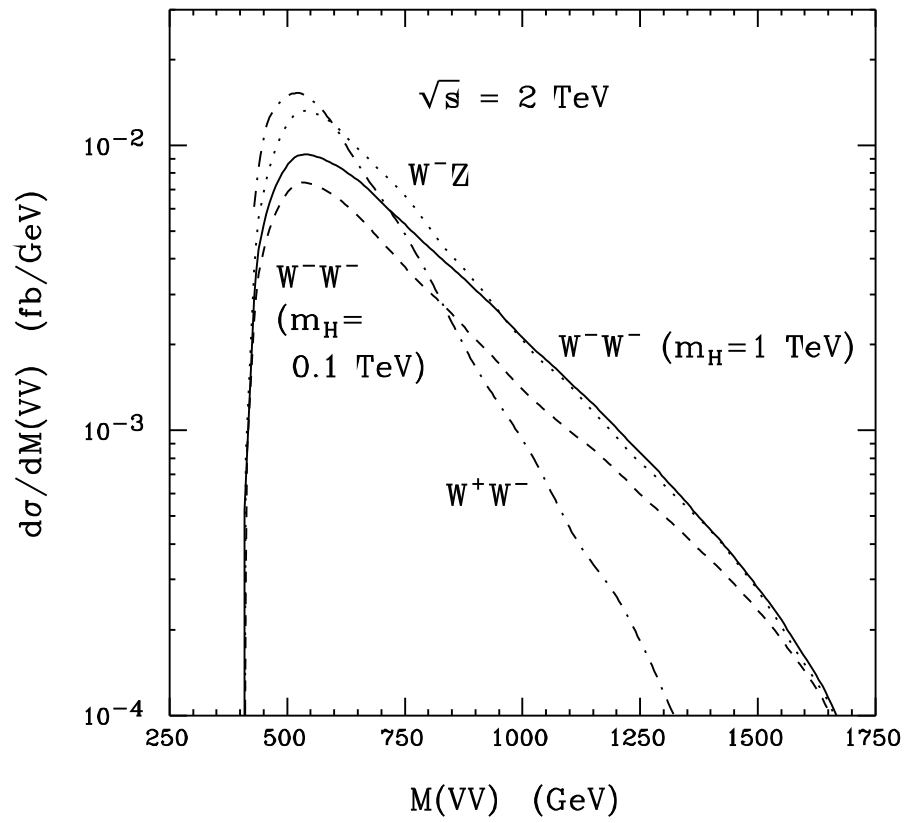


Fig. 9

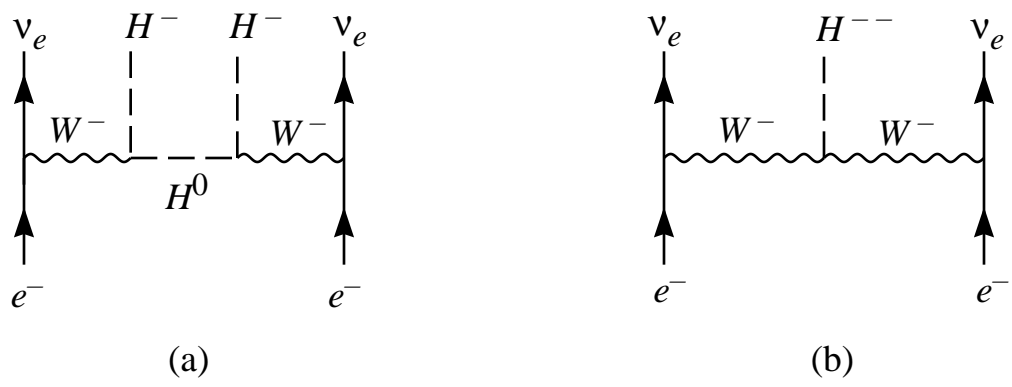


Fig. 10

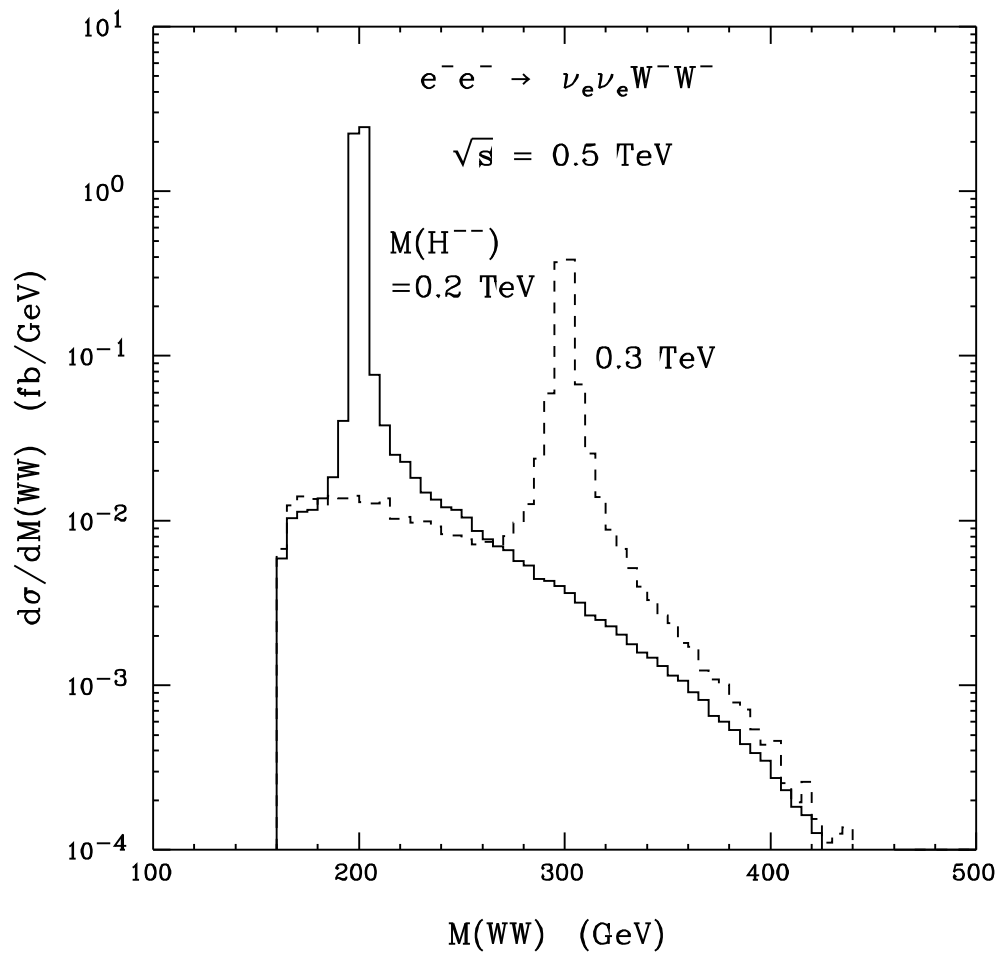


Fig. 11